The Evolution and Dynamical Role of Reduced Upper-Tropospheric Potential Vorticity in Intensive Observing Period One of FASTEX

HANNAH R. POMROY AND ALAN J. THORPE

Department of Meteorology, University of Reading, Reading, United Kingdom

(Manuscript received 4 February 1999, in final form 8 June 1999)

ABSTRACT

The existence and production of reduced upper-tropospheric potential vorticity (RUPV) by heating is considered. An objective technique is used that identifies anomalies of PV arising from a particular physical process (here latent heat release). The evolution of two RUPV anomalies and a related diabatically increased lower-tropospheric PV (ILPV) anomaly occurring during Intensive Observing Period One of the cyclones from the Fronts and Atlantic Storm Track Experiment (FASTEX) is examined using model analyses, sounding data, and trajectory calculations. Three distinct airflows are identified emanating from the ILPV anomaly each with a different evolution. Results show that RUPV anomalies exist in the atmosphere and, in a weaker form, in numerical models.

The dynamical role of RUPV anomalies is examined using a nonlinear balance PV inversion and reruns of the U.K. Meteorological Office Limited Area Model. This shows that instantaneously the flow and temperature perturbations associated with RUPV anomalies are of at least comparable magnitude and extent to those induced by a similar positive anomaly. Over time one RUPV anomaly is seen to have a significant effect upon the development of its parent low. This low is more compact and more rapidly developing in the absence of the anomaly. The effect of the positive anomaly is also significant, but removing it has only a short-term effect as the anomaly quickly reforms. These results show that it is important to consider the role of RUPV in the PV model of a midlatitude cyclone.

1. Introduction

Despite being a dominant topic of meteorological research for more than a century, the forecasting of midlatitude depressions still provides many unanswered questions. Although numerical prediction models continue to increase their computational power it is important to match this with greater conceptual understanding of extratropical cyclones. This is needed to improve the parameterizations used for physical processes, to reconcile theory and observations, to optimize the location and type of observations, and to add value to the numerical output.

An important tool making a significant contribution toward this extension is ''potential vorticity thinking,'' which provides a unifying framework within which to consider the complex development of a cyclone. Potential vorticity (PV) is conserved in adiabatic, frictionless flow, and is invertible under specific conditions. However PV can be created and destroyed by friction, and diabatic processes. Anomalies of PV exist as telltale markers of these nonconservative processes. It can therefore be said that PV encapsulates all midlatitude dynamics in a single scalar quantity. The Lagrangian rate of change of potential vorticity is given by

$$\frac{D}{Dt}P = \frac{1}{\rho}\left[\zeta \cdot \nabla\left(\frac{D\theta}{Dt}\right) + \nabla \times \mathbf{F} \cdot \nabla\theta\right], \qquad (1)$$

where $P = (1/\rho)\boldsymbol{\zeta} \cdot \nabla\theta$ = potential vorticity, θ = potential temperature, $\boldsymbol{\zeta}$ = absolute vorticity, ρ = density, and $\mathbf{F}$ = friction. The first term on the right-hand side represents changes in PV due to diabatic processes, and the second term is due to frictional processes. On the whole frictional processes are small away from the boundary layer. The rate of change of PV is therefore primarily a function of the gradient of the rate of change of potential temperature.

A parcel of air advected from below through a region of latent heat release will encounter a region of PV generation.[1] On passing through the level of maximum rate of change of potential temperature the gradient of

Corresponding author address: Alan J. Thorpe, Hadley Centre for Climate Prediction and Research, Meteorological Office, London Road, Bracknell, Berkshire RG12 2SY, United Kingdom.
E-mail: ajthorpe@meto.gov.uk

[1] The maximum PV modification will occur parallel to the absolute vorticity vector. Here, for the purposes of illustration, it is assumed that this vector is approximately vertical, which is usually true on the synoptic scale.

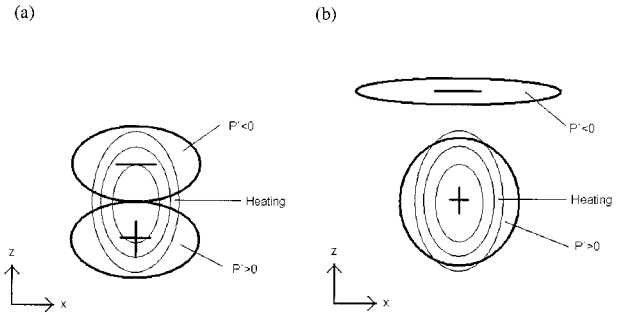

FIG. 1. (a) Impulsive heating source; (b) steady-state heating source (adapted from Wernli 1995).

heating becomes negative, and a region of PV destruction exists. This argument implies that instantaneously a positive PV anomaly below the level of maximum heating (known here as increased lower-tropospheric PV, or ILPV) and a negative anomaly above (reduced upper-tropospheric PV, or RUPV[2]) will exist. When the heating is steady state, that is, continues over time periods of the same order as the vertical advection, the positive anomaly is collocated with the heating maximum and the negative anomaly advected away, or dispersed to infinity. This is represented schematically in Figs. 1a and 1b, respectively.

These ideas of ''instantaneous'' and ''steady state'' represent extreme models of idealized states encompassing the range of possibilities. Considerations such as nonsymmetric heating patterns, unsteady heating rates, and air motion in other directions are ignored. The instantaneous model was developed by Kleinschmidt (1950; see also Haynes and McIntyre 1987, 1990; Hoskins 1991), and the steady-state model by Wernli (1995; see also Wernli and Davies 1997). Evidence to support this latter model is supplied by Persson (1995) and Stoelinga (1996).

Significant conceptual advances have been made by considering the positive low-tropospheric PV anomaly due to heating within the center of a cyclone, augmenting the wavelike signatures in the upper-level PV field, and the surface thermal field (e.g., Davis and Emanuel 1991; Davis 1992; Davis et al. 1993; Stoelinga 1996). However very little research has been undertaken on the existence and role of diabatically produced negative PV anomalies. Regions of abnormally low PV have been observed in the upper troposphere and some previous investigations suggest they play an important role in extratropical cyclone genesis and development. Development of new diagnostic techniques including attribution ideas (Bishop and Thorpe 1994; Thorpe and Bishop 1995) and the improvement of data collection provides new avenues for research in this area. A hindrance has been the ambiguity and poor definition of low PV as anomalous. Although its theoretical existence has long been known and discussed, its existence in real cyclones is unclear. In addition to the dynamical significance of these features, attention should be paid to these ''anomalies'' even if just for ''completeness'' with respect to the related positive diabatic anomaly. Without a better knowledge of its characteristics, evolution, and power, our conceptual PV picture of a cyclone is incomplete.

The aim of this paper is to reduce this gap in understanding by considering the following questions:

- How does reduced upper-tropospheric PV evolve?
- How important is reduced upper-tropospheric PV in midlatitude cyclone genesis and evolution, particularly in comparison to increased lower-tropospheric PV anomalies also created by diabatic processes?
- Is the presence of RUPV within numerical model analyses validated by atmospheric soundings?

The paper is structured as follows. A brief introduction to the tools used for the work will be presented in section 2, followed in section 3 by a discussion of the synoptic characteristics of the case study to be used. Section 4 will present an analysis of two RUPV anomalies identified within the case study. Section 5 is an equivalent analysis for an ILPV anomaly within the same case study. Finally in section 6 the implications of the results from the previous two sections will be discussed.

2. Methodology

An anomaly of PV will be identified within case studies using an objective definition. Trajectory information will be used to determine the history of the air residing within that anomaly. The PV anomaly will be inverted to determine the fields of wind and potential temperature directly attributable to it. Two runs of the U.K. Meteorological Office Limited Area Model (LAM) will be compared, the first initialized by the inverted fields from the full PV and the second initialized by the inverted fields from the PV field minus the PV anomaly. This will examine the temporal influence of the PV anomaly on the atmospheric system. Finally any relevant observations of the anomaly will be considered.

The data used throughout the case study, unless otherwise stated, are obtained from the U.K. Meteorological Office model analyses. These are verified analyses at 0000, 0600, 1200, and 1800 UTC, and model 3-h forecasts at 0300, 0900, 1500, and 2100 UTC. (Caution must therefore be used when considering results deduced on evidence solely from forecast times.) The model used is the regional forecast model or LAM with domain including the eastern United States and Canada, the North Atlantic Ocean, Europe, and the Mediterranean (Cullen 1993). The grid used has resolution of

[2] The term RUPV means that the product of the Coriolis parameter times the PV is smaller, and can even become negative, relative to typical values at that location.

0.44° (~50 km) and is a spherical rotated latitude–longitude grid with the pole at 30°N, 160°E. The adjustment time step is 100 s, the advection time step 300 s, and the physics time step 900 s. There are 19 levels in the vertical at around 1000, 950, 925, 850, 700, 500, 400, 300, 250, 200, 150, 100, 70, 50, 30, 25, 20, 15, and 10 hPa.

To define each PV anomaly objectively a new technique has been developed. This aims to address a particular criticism of past methods that they are unable to objectively identify an anomaly produced by a specific process, in this case latent heating. Our technique can be summarized as follows:

1) Define a box enclosing the ''suspected'' anomaly large enough to remove bias.
2) Perform back-trajectory analysis from the box to determine the history of the air parcels contained within it.
3) Calculate the latent heat release along individual trajectories.
4) Isolate the trajectory endpoints within the initial box for which the total heating along the trajectory is greater than zero.
5) Replace the PV at these endpoints with the PV at an earlier time along the corresponding trajectory. The time when the PV of the air parcels was approximately conserved, prior to modification by diabatic processes, is chosen as the earlier time. It is important to note that the replacement of the PV at the endpoint of a trajectory with the PV at an earlier time along the trajectory is arbitrary.
6) Subtract the initial PV field from the new PV field to determine the anomalous PV.

The trajectory calculation estimates the location of the air parcel at the next time step using the wind at its initial position, and then using the average of the winds at this estimated next location and at the initial location, advects the parcel forward. A time step of 15 min is used for data with a temporal resolution of 3 h. This method was adapted by Wernli (Wernli and Davies 1997) from Petterssen (1956), and is similar to the methods used by Whitaker et al. (1988), Kuo et al. (1992), and Reed et al (1992). (See also Seibert 1993.) The latent heat release is calculated using the rate of change of specific humidity along the trajectories, and specifying that the relative humidity should be greater than 80%, and ascent occurring.[3]

A PV inverter is employed to determine both the fields due to the anomaly and the initialization fields for the rerun. This inverter is based on the nonlinear balance approximation to the potential vorticity. By assuming that the irrotational flow is smaller in magnitude than the nondivergent flow, and that divergence and its time tendency are small in the divergence equation, two equations are obtained that when written in the Exner vertical coordinate system are

$$P = \frac{gK\pi}{p}[(f + \nabla^2\psi)\phi_{\pi\pi} - \psi_{x\pi}\phi_{x\pi} - \psi_{y\pi}\phi_{y\pi}] \quad (2)$$

and

$$\nabla^2\phi = \mathbf{\nabla} \cdot (f\mathbf{\nabla}\psi) + 2(\psi_{xx}\psi_{yy} - \psi_{xy}^2), \quad (3)$$

where P = PV, ϕ = geopotential, ψ = streamfunction, $K = R/c_p$, and $\pi = c_p(p/p_0)^K$. By multiplying (2) by a suitable factor and combining the resulting equation with (3), two simultaneous equations are obtained for ϕ and ψ. A process of inversion and iteration solves these, until the original equations, (2) and (3), are satisfied to within 0.05 PVU and 0.05 f, respectively. The boundary conditions that are used are as follows:

- potential temperature on the top and bottom boundaries is specified,
- $\partial\phi/\partial\pi = -\theta$ is specified on the vertical boundaries,
- and ψ is defined on the lateral boundaries such that the total divergence over the whole domain is zero; that is,

$$\frac{\partial\psi}{\partial s} = -\mathbf{v} \cdot \mathbf{n} + \frac{\oint \mathbf{v} \cdot \mathbf{n}\, dl}{\oint dl},$$

where l is a path around the surface that encloses the domain, s is a tangent to that path, and $\mathbf{n}$ a normal to that path.

This method is very similar to that employed by Davis and Emanuel (1991). [This inverter has been developed by M. Ziemianski and M. Demirtas, and extended by M. Griffiths. Further information on it can be found in Ziemianski (1994), Demirtas and Thorpe (1999), and Griffiths et al. (1999).] The full LAM area cannot be inverted as the NAG routines employed by the nonlinear balance inverter have a restriction on the number of data points included. This means that a subsection of the domain must be prescribed centered on the feature of interest to ensure that the boundary conditions, and less accurate finite differencing schemes used there, do not impact significantly on any conclusions drawn from the inversion. After inversion the fields derived are extended to the full size of the domain with the original fields outside the subdomain.

To obtain the fields due solely to the PV anomaly two inversions are performed. The first is on the full PV field to calculate the nondivergent (or rotational) component of the wind and the potential temperature

[3] At a point latent heating will only occur when the air is saturated. This criterion is relaxed within the Unified Model to greater than 85% relative humidity with respect to water, to account for the resolution and accuracy of the physics schemes. Here 80% is chosen to account for ice saturation lowering this threshold further at upper levels.

fields. The second inversion is performed on the full PV field minus the PV anomaly (the modified PV). Then the results are subtracted to find the field due to the PV anomaly. In this way the effect of the environmental PV upon the anomaly can be accounted for. The division of the PV field thus, effectively into two anomaly fields, can be justified following the results of Birkett and Thorpe (1997). Their experiments show that the fields that PV anomalies induce can be quasi-linearly superposed when the anomalies are spatially distinct. Subtracting the fields due to the full PV from those due to the modified PV field leaves only the flow and potential temperature signature attributable to the PV anomaly. Any finescale structure in the ''new'' PV field is not present in the inverted fields.

3. Case study description: FASTEX IOP 1

The Fronts and Atlantic Storm Track Experiment (FASTEX) took place during January and February 1997 (Joly et al. 1997). A principal aim of the experiment was to observe in detail the mesoscale structure of cyclonic storms across the North Atlantic Ocean. This was achieved using ships, aircraft deployed specifically, and additional radiosonde launches from the conventional observation network. Summaries of the principal features of each intensive observing period (IOP) undertaken are given in Clough et al. (1998).

The frontal wave appearing in the mid–North Atlantic on 9 January 1997 was the subject of the first IOP of FASTEX. The cyclone developed from a short wave orientated north–south along the eastern flank of a pronounced upper-level ridge–trough pattern. Initially two, and then three, other cyclones were associated with this trough and the situation was described at the time as a ''complex low,'' the low centers appearing to revolve around each other. Low 8a, the subject of IOP 1, was the least significant of the lows, but initial forecasts indicated rapid development and a good example of a frontal wave cyclone. However the development of the low was in some way constrained and although it tracked northward into the mesoscale sampling area (MSA), it did not develop explosively and, in fact, decayed rapidly on entering the MSA. At its peak the wave cyclone reached a minimum pressure of 985 hPa, and had an estimated system velocity of 22 m s^{-1}. The wave cyclone exhibited both a primary and a secondary standard surface warm front, while a primary cold front could be objectively analyzed both at the surface and at upper levels. A double cloud-head structure can be clearly seen in the satellite imagery and a distinct dry slot was also observed.

Model ''analyses'' show two regions of unusually low and negative PV in the vicinity of the maturing cyclone. Their location in relation to the cyclone can be seen in Fig. 2a. Low 8a is the smallest closed contour at 54°N, 20°W, the fourth developing cyclone lies to the southwest of it (not shown). Low 10, the subject of FASTEX lesser observing period one (FLOP 1) is also marked. (The development of these two lows can be followed in Fig. 10.)

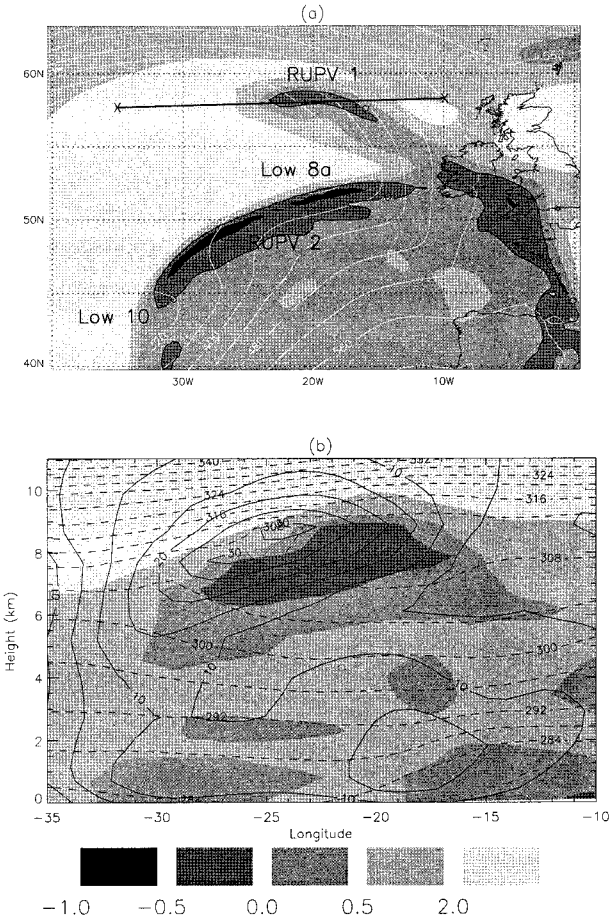

FIG. 2. (a) Shading: potential vorticity at 300 hPa at 0600 UTC 10 Jan 1997; contours: 950-hPa geopotential height, contour interval 40 m. Line marks position of cross section in (b). (b) Vertical cross section at 57°N through RUPV 1. Shading: potential vorticity (minimum value = −0.2 PVU); solid line: southerly wind component (contour interval: 5 m s^{-1}); dashed line: potential temperature (contour interval: 4 K).

4. Analysis of the RUPV anomalies in IOP 1

a. RUPV 1

Reduced upper-tropospheric PV one (RUPV 1) is closely associated with low 8a. This region of reduced PV developed to the north and downstream of the surface low, at around 350 hPa. Using the trajectory technique described above, the anomaly is defined at 0300 UTC on 10 January 1997. The details of the anomaly definition are shown in Table 1. The anomaly has extremum amplitude of 0.72 PVU. It is marked in Fig. 2a 3 h later and a cross section through the anomaly at that time is shown in Fig. 2b. This figure also shows the structure of the potential temperature and wind in the

TABLE 1. The first three rows indicate the dimensions of the boxes used as part of the process to define each anomaly (anomaly definition technique step one). The fourth row shows the earlier time chosen to determine the strength of PV modification (anomaly definition technique step five). The fifth row shows the total number of trajectories emanating from the anomaly.

	RUPV 1	RUPV 2	ILPV 1
Pressure depth	500–250 hPa	400–200 hPa	900–450 hPa
Meridional bounds	14°–28°W	10°–34°W	25°–40°W
Zonal bounds	53.5°–58.5°N	41°–53°N	42°–48°N
''Earlier'' time	0900 UTC 9 Jan 1997	0600 UTC 9 Jan 1997	1200 UTC 8 Jan 1997
Total no. of trajectories	271	893	1005

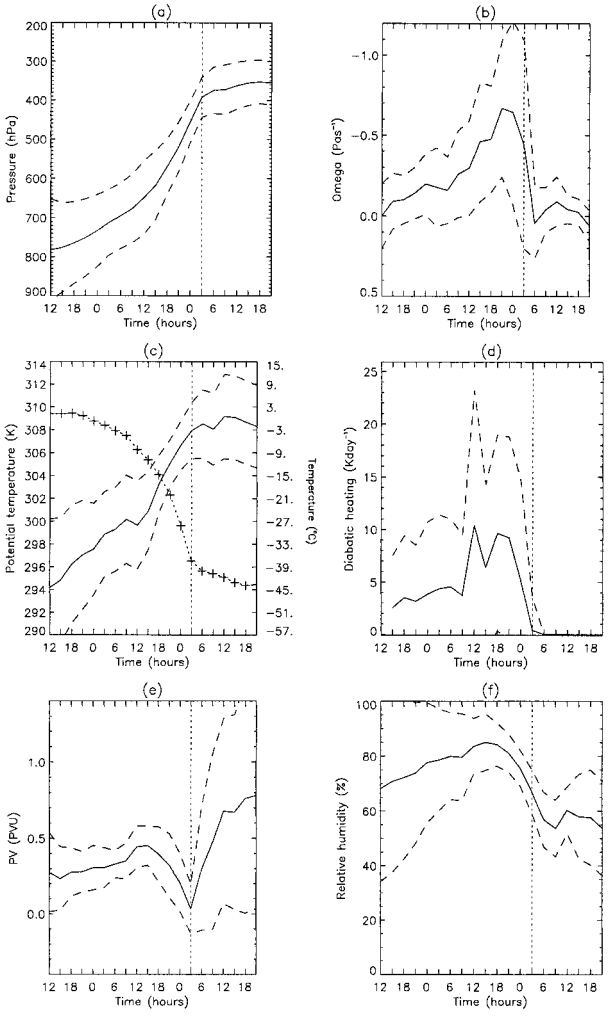

FIG. 3. Solid lines: characteristics of average trajectory experiencing heating and emanating from RUPV 1. The anomaly definition time is 0300 UTC on 10 Jan 1997 marked by the small dashed vertical line in each graph. The trajectories are calculated from 1200 UTC on 8 Jan to 2100 UTC on 10 Jan (a) Pressure (hPa); (b) vertical velocity (Pa s^{-1}); (c) solid line, potential temperature (K); dashed line with crosses, temperature (°C); (d) heating (K day^{-1}); (e) potential vorticity (PVU); and (f) relative humidity (%). Abscissa shows time from 1200 UTC 8 Jan 1997 to 2100 UTC 10 Jan 1997. Dashed lines following trajectory curves show one standard deviation from the average.

region of the anomaly. Note the negative static stability within the anomaly, and the strong jet in the wind at the tropopause.

1) EVOLUTION

The anomaly RUPV 1 has been defined by its source of PV being latent heating occurring during the life of low 8a prior to 0300 UTC on 10 January. A set of trajectories has been identified that describes the path of each air parcel belonging to RUPV 1 at 0300 UTC on 10 January, over the previous 39 h. These trajectories are also extended forward for 21 h from 0300 UTC on 10 January for this study.

To provide insight into the variation of the properties of the air parcel, Fig. 3 shows how the properties of the average trajectory vary with time. These properties are calculated by simply summing each characteristic (e.g., PV, temperature) at a particular time for all the trajectories, and dividing by the total number of trajectories. Figure 3 also includes a measure of the dispersion of the trajectories around the average at each time, namely the plus and minus one standard deviation lines from the mean. Statistically, around 68% of the air parcels belonging to the trajectory ensemble reside within these two lines.

Figure 3a shows that on average the trajectories begin at around 800 hPa. At this ''initial'' time they are relatively moist but have no significant diabatic source (Figs. 3d and 3f). As shown later, in the horizontal the parcels at the beginning are spread out in a long band in the lower troposphere, along a front and also have significant spread in the vertical. By 0300 UTC on 9 January the parcels are gradually converging toward the center of the developing low. At this time the cyclone is at around 43°N, 45°W and the majority of the air parcels are slightly ahead of the 950-hPa low center indicating the position of the zone of maximum ascent ahead of the low. The decrease in potential temperature over time of the parcels is approximately constant and this is reflected in the consistency in the amount of diabatic heating (Figs. 3c and 3d). At this time the air parcels are horizontally compact and distributed more in the vertical. They rapidly ascend (at approximately -0.35 Pa s^{-1}), through the main region of latent heat release as indicated by the highest relative humidities (Fig. 3f). The maximum in heating leads the maximum

in vertical velocity by 3 h, although the double peak in diabatic heating confuses this signal. This lag in the maximum ascent is expected as higher temperatures near the surface weight the maximum potential for moisture release toward the lower troposphere. The maximum in vertical velocity, a second factor in the magnitude of the heating, lies higher up in the midtroposphere (approximately 500 hPa here). These two factors balance to give a maximum in heating higher than the maximum relative humidity but lower than the maximum vertical velocity.

Between 1500 UTC on 9 and 0300 UTC 10 January the parcels ascend over 250 hPa on average, suffer a sharp drop in specific humidity to almost zero, and undergo the maximum heating. They are compact as they perform this rapid ascent, but experience large variations in diabatic heating and vertical velocities. At 0300 UTC on 10 January the parcels reside in RUPV1, north of the low center in the outflow from the main ascending region. The pressure is on average 375 hPa, which is just below the tropopause. No more heating occurs, and the parcels reach an ''equilibrium'' in temperature, specific humidity, and pressure for the last 18 h.

The changes in the PV of the average trajectory correspond to these changes in the other trajectory characteristics. The average evolution of the PV over time is shown in Fig. 3e. It can be seen that the average parcel begins with a typical lower-tropospheric PV of around 0.25 PVU. A gradual increase in this value is seen as the parcels rise up and it reaches a peak in PV at 1500 UTC on 9 January of 0.5 PVU. This is at approximately the same time as the highest value of diabatic heating occurs (Fig. 3d). Since a double maximum in heating is seen it is unclear as to the exact relationship in time of the maximum heating to the maximum PV. Subsequent to the peak in the average PV value, a sharp drop is seen (Fig. 3e) to a minimum of 0.03 PVU at 0300 UTC on 10 January. This is significantly lower than the average value of PV the parcels began with, and occurs at a time when the parcels have stopped ascending and the influence of latent heat release has ceased.

During the final 18 h of tracking the air parcels, although all the other parameters remain roughly constant, the PV of many parcels increases rapidly to a value much larger than the latent heat release induced peak. Note the larger standard deviation in PV during this period. Possible mechanisms for this PV increase include turbulent PV production in the jet stream or, perhaps, more likely the trajectory position error near the strong PV gradients at the tropopause. Further examination of these issues is beyond the scope of this paper.

2) INVERSION

The PV field after the removal of the anomaly RUPV 1 can be seen in Fig. 4a. Figure 4b shows the resulting anomaly when this field is subtracted from the full PV field. Note that the apparently anomalous region is not entirely absent in Fig. 4a. This implies that the objective technique has not removed all the low PV within the ''suspected'' anomaly. This shows that advection from well within the troposphere also accounts for some of the low PV.

Figures 4c and 4b show these fields in vertical cross section with the position of the tropopause (PV = 2 PVU) and the outline of the anomaly also marked on. Figure 4c shows the potential temperature perturbations due to RUPV 1 along a meridional section. Table 2 shows the maximum values of the fields induced for each anomaly. It also shows a measure of the relative magnitude of the fields induced. This is calculated by finding the range in the full wind and potential temperature fields at the appropriate levels within the inverted region. The percentage of this range that can be attributed to the anomaly is then calculated.

The signature of warmth below the anomaly and a cold region above the anomaly is characteristic of a negative anomaly. In addition the warmth below the anomaly is less than the cold above and penetrates less far away from the anomaly. This agrees with the dependence, in theoretical models, of the induced potential temperature perturbation on the presence of the tropopause (Birkett 1998). The higher PV in the stratosphere above the anomaly acts to increase the perturbation in potential temperature and also increase the penetration of the perturbation into the stratosphere. In fact the high PV of the stratosphere surrounds RUPV 1 everywhere except beneath it.

Figure 4d shows the equivalent velocity field along a zonal plane associated with the anomaly. The effect of the tropopause on the wind field is even more pronounced. The wind anomaly has hardly any penetration into the stratosphere despite the anomaly residing so close to it. Again this observation agrees with theoretical results. The figure shows the characteristic anticyclonic circulation that one would expect to see around a negative anomaly. The wind also shows the concentration of the flow into a ''jet'' around the edge of the anomaly where the PV gradient is steep.

3) RERUN

To calculate the atmospheric response to the anomaly RUPV 1 defined at 0300 UTC on 10 January, two model forecasts were generated. The first of these was a rerun of the LAM from 0000 UTC on 10 January, stopped at 0300 UTC, and restarted with the fields from an inversion of the full PV field. The second was restarted using fields from the inversion of the PV field generated by removing objectively defined RUPV 1. A subarea of this field at 300 hPa is illustrated in Fig. 4a. The results show a maximum of 0.9% difference between the geopotential height field of the full PV forecast and the geopotential height field of the modified PV field forecast. This maximum difference oc-

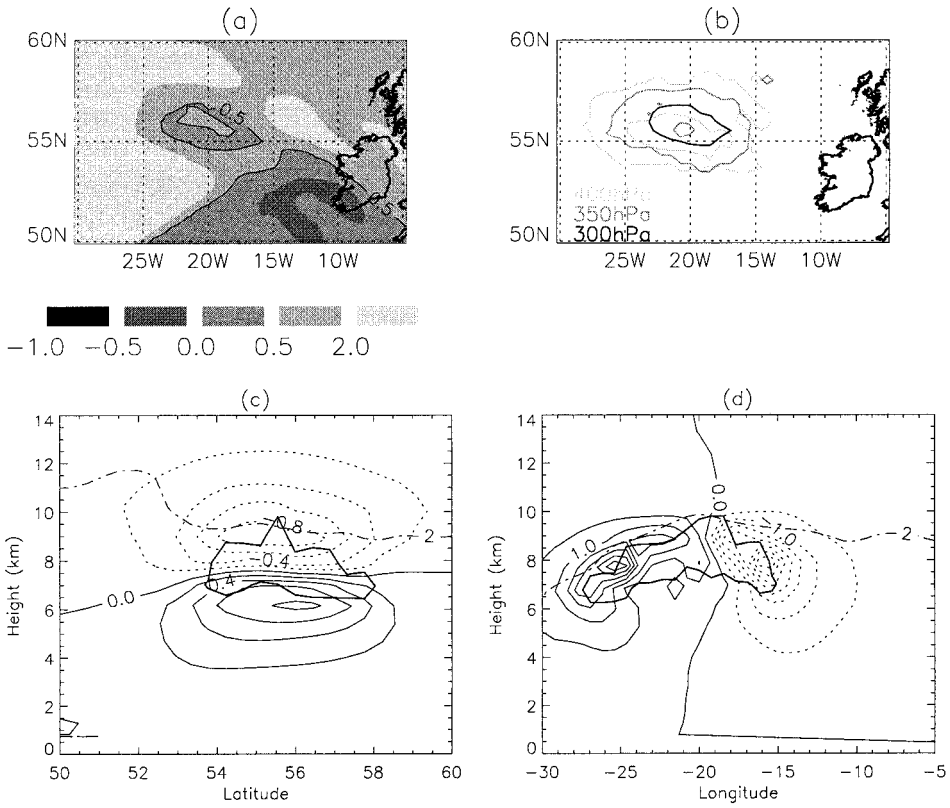

FIG. 4. (a) The PV field after surgery to remove RUPV 1 at 300 hPa at 0300 UTC 10 Jan 1997, (b) −0.1 PVU contour outlining position of PV anomaly. Light gray, 400 hPa; dark gray, 350 hPa; black, 300 hPa. (c) Vertical cross section through anomaly induced potential temperature perturbation at 20°W (contour interval = 0.2 K; positive contours, solid; negative contours; dashed). (d) Vertical cross section through anomaly induced model v component at 55.1°N (contour interval = 0.5 m s^{-1}; positive contours, solid; negative contours, dashed). Bold contour: anomalous PV field = −0.1 PVU. Dotted–dashed contour: PV = 2 PVU contour for unmodified data.

curs at 900 hPa at 1500 UTC on 10 January, 12 h after reinitialization. Low 8a decays at the same rate in both reruns, and the forecasts closely follow the analysis data. Further latent heat release within the anomaly does not reform RUPV 1.

4) OBSERVATIONS

The U.K. C-130 aircraft flew through low 8a from 0000 to 1200 UTC on 10 January 1997. It released dropsondes in lines to create cross sections of the main features of the depression, and also gathered data at the flight level (~7.9 km). On the whole the LAM analyses agree well with these flight-level observations in structure although the measured temperatures are a few degrees higher than the model in general. The aircraft is also able to pick out small-scale structure in the wind field that the model misses.

TABLE 2. Results from inversion of anomalies. The range is defined as the maximum difference of that field within the inverted box.

	Max anomaly magnitude (PVU)	Max potential temp. anomaly induced (K)	Max wind anomaly induced (m s^{-1})	Anomaly to range of potential temp. (%)	Anomaly to range of wind (%)
RUPV 1	−0.72	1.03	6	5	12
RUPV 2	−2.12	1.35	7.2	7	13
ILPV 1	0.72	0.88	3.4	4	10

A reduced PV signature is seen in data from dropsondes released during the second and third aircraft runs, from 56.2°N, 23.3°W to 55.4°N, 23.9°W, and from 55°N, 24.1°W to 54.6°N, 19.8°W, respectively, between 0500 and 0700 UTC. These also display a distinctive feature occurring variously between 500 and 380 hPa. For example sounding 17, taken at 54.6°N, 21.4°W, shows a profile characteristic of the stratosphere with very dry, statically stable air between 480 and 470 hPa. Figure 5 shows a tephigram of this sounding. The solid lines indicate the temperature profile, and the dewpoint temperature is shown in dashed lines. The wind direction and speed are marked on the right-hand side, direction in the left-hand column of numbers, speed in knots in

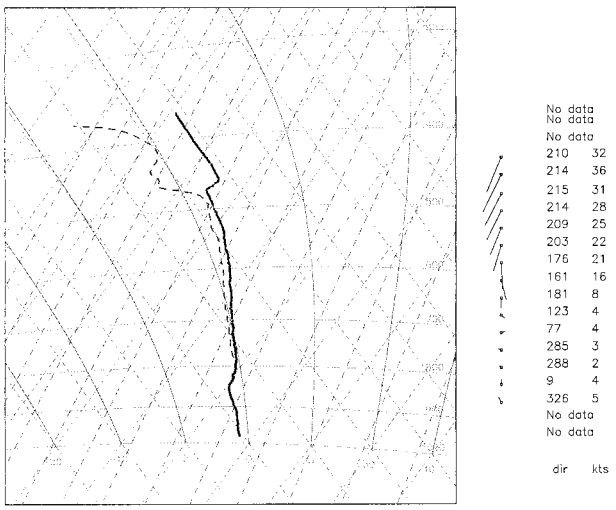

FIG. 5. Tephigram of dropsounding 17 taken at 0558 on 10 Jan 1997, from U.K. C-130, at 54.6°N, 21.4°W. Atmospheric temperature is marked by a solid, bold line and the dewpoint temperature by a dashed line. Winds are shown on the right-hand side of each tephigram, the first column contains the direction, and the second the speed in kt.

the right-hand column. Where no wind data are available from the sounding, this is marked accordingly. Above the tropopause at 470 hPa the profile once again becomes characteristic of the troposphere, with moist air, and an almost neutral environmental lapse rate. The pattern is recognizable therefore as a stratospheric intrusion or tropopause fold. Above the fold the air has such low stability that regardless of the vorticity signature the PV at this level must be very small.

b. RUPV 2

A ''streamer'' of low PV can be seen running along the eastern flank of the pronounced upper-level trough, just below the tropopause, throughout the development of low 8a. Although this streamer remains at a constant magnitude, it is quite broken at times, and coherent at others. At 0600 UTC on 10 January there is a marked decrease in the PV magnitude at 300 hPa slightly upstream of the surface low, and a long, thin region of anomalously low PV (RUPV 2) can be objectively identified (see Fig. 2). It has minimum magnitude of -2.12 PVU that is indicative of the very low PV values in this region at this time. The details of the anomaly definition process are shown in Table 1.

1) EVOLUTION

To illustrate the properties of the RUPV 2 air parcels, Fig. 6 displays the average characteristics of the trajectories and the deviation around that mean. As before the dashed lines mark one standard deviation within which 68% of the air parcels reside. From this it can be seen that the air parcels begin at around 800 hPa at

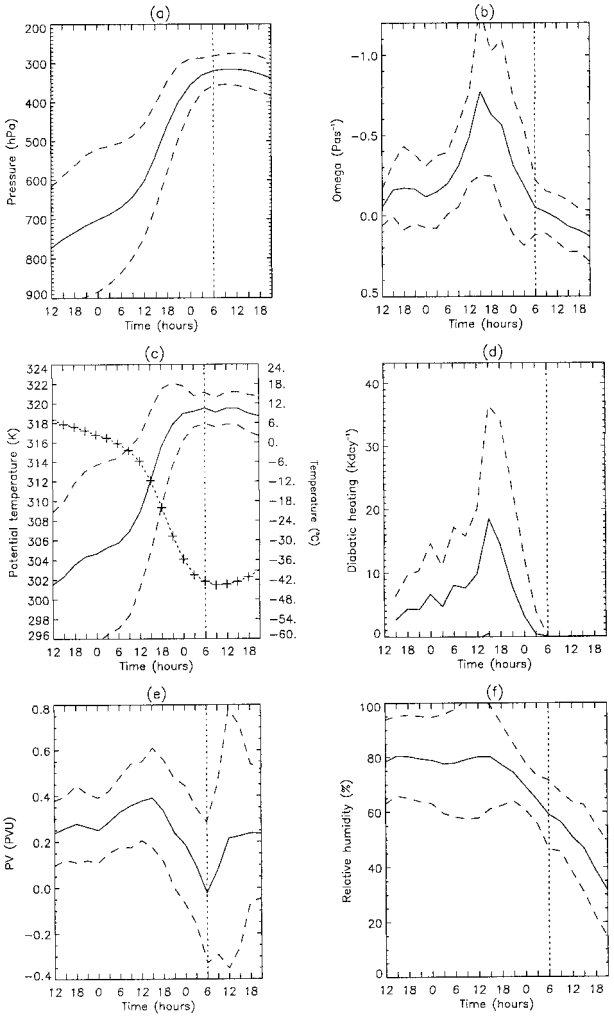

FIG. 6. Solid lines: characteristics of average trajectory experiencing heating and emanating from RUPV 2. The anomaly definition time is 0600 UTC on 10 Jan 1997 marked by the small dashed vertical line on each graph. The trajectories are calculated from 1200 UTC on 8 Jan to 2100 UTC on 10 Jan; (a) pressure (hPa); (b) vertical velocity (Pa s^{-1}); (c) solid line, potential temperature (K); dashed line with crosses, temperature (°C); (d) heating (K day^{-1}); (e) potential vorticity (PVU); and (f) relative humidity (%). Abscissa shows time from 1200 UTC 8 Jan 1997 to 2100 UTC 10 Jan 1997. Dashed lines following trajectory curves show one standard deviation from the average.

1200 UTC on 8 January. At this stage they have a PV signature typical of the lower troposphere, on average 0.25 PVU. On the basis of wet-bulb potential temperature analyses (not shown) there appear to be two separate air until around 0600 UTC on 9 January, but they merge by 1800 UTC on 9 January. This is also reflected in the larger variance in some of the trajectory characteristics shown in Fig. 6. In comparison to RUPV 1 the motion of the air parcels involves a larger average maximum vertical velocity, a greater amount of time spent in very moist air, a greater fall in specific humidity, and undergoing, on average, considerably more heating.

The peak in heating occurs at 1500 UTC on 9 January when the air parcels are predominantly influenced by processes occurring within the developing secondary low (low 10; see Fig. 2), upstream of low 8a. The airstream moves rapidly through the heating region and emerges higher up than RUPV 1, at around 300 hPa. During the latent heat release, the air parcels gain around 0.15 PVU, less than RUPV 1, peaking at the same time as the heating maximum. Subsequently a sharp, rapid drop in the PV magnitude is recorded of more than 0.4 PVU on average, to give a negative mean PV value. The air parcels are spread out along the midlatitude tropopause cliff, south of the low center. They remain between 300 and 400 hPa for the final 18 h of analysis and follow the jet stream southward away from decaying low 8a. A rapid average increase in the PV of the air parcels is seen over the first 6 h after 0600 UTC, as for RUPV 1, but the increase returns the PV to the value it began with at 1200 UTC on 8 January. Notice that again there is a larger spread of PV values during the period parcels are close to the tropopause.

2) INVERSION

The PV field after the removal of the anomaly RUPV 2 can be seen in Fig. 7a. Figure 7b shows the resulting anomaly when this field is subtracted from the full PV field. Figures 7c and 7d show these fields in vertical cross section with the position of the anomaly outlined by a bold line. Table 2 shows the maximum magnitude of the fields induced by the anomaly. Figure 7c shows the potential temperature perturbations due to RUPV 2 in a longitudinal section. Again the characteristic signature of warmth below the anomaly and a cold region above the anomaly is seen. The magnitudes of these two temperature anomalies are almost identical unlike for RUPV 1. This may be accounted for by the proximity of the stratosphere; RUPV 1 is surrounded by it on three sides whereas RUPV 2 lies clearly within the troposphere.

Figure 7d shows the equivalent velocity field attributed to the anomaly. The component of the wind in an approximately northerly direction is shown. As expected an anticyclonic flow is seen around the anomaly. The effect of the tropopause on the magnitude of the wind field is again more difficult to detect than for RUPV 1, although it can be seen that there is very little vertical penetration into the stratosphere. The wind again shows a concentration of the flow into a ''jet'' around the edge of the anomaly and particularly on the northwest flank of the anomaly where it is adjacent to a steep tropopause cliff, the large horizontal gradient in PV inducing the strongest flows.

3) RERUN

To calculate the atmospheric response to the anomaly RUPV 2 defined at 0600 UTC on 10 January, two model forecasts were generated. The first of these was a direct rerun of the LAM from 0600 UTC on 10 January, initialized with the fields from an inversion of the full PV field. The second was initialized using fields from the inversion of the PV field generated by removing objectively defined RUPV 2. A subarea of this field at 300 hPa is illustrated in Fig. 7a.

The maximum difference in geopotential height between the two forecasts occurs at the lowest levels and increases in time from around 3% difference at initial time. This would be expected from diverging forecasts. At 950 hPa at 0000 UTC on 11 January the negative maximum is 7.7%. This value reflects the fact that the upstream low, low 10, is much tighter and farther advanced toward the British Isles by this time in the modified PV forecast than the full PV. This creates a dipole of lower and higher geopotential heights where the low is displaced between forecasts. A larger negative geopotential height anomaly indicates that the low is smaller in extent, and less deep in the modified forecast. Differences in the development of low 10 are the main disparities between the two runs. Its initial development is suppressed in the modified PV forecast, while very little variation is seen in the development of low 8a. Between 1200 and 1500 UTC low 10 develops rapidly in the second run, developing farther to the northeast and more compactly than for the full PV run. Comparison of the two 300-hPa geopotential height fields shows that there is a small reduction in the anticyclonic flow, and therefore anticyclonic curvature, of the upper-level ridge. Consequently the trough is also slightly stronger and broader, extending farther east in the modified PV forecast by approximately 400 km, giving a geopotential height difference of up to 25 m at 300 hPa. A snapshot of these results at 0000 UTC ($T + 18$) on 11 January 1997 is shown in Fig. 8. The top row shows the 300-hPa geopotential height fields for (a) the full PV forecast, (b) the modified PV forecast, and (c) the difference between these two fields, and on the middle row the same fields at 950 hPa. The bottom row shows as schematic of the changes (discussed in section 6).

As for RUPV 1, RUPV 2 does not redevelop in the second run, but a new RUPV anomaly does develop in the upper troposphere and pushes up the stratosphere in both forecasts as a product of low 10. This anomaly is similar in relative location and magnitude to RUPV 1 within low 8a.

4) OBSERVATIONS

No flights were made through the region of RUPV 2, but several weather ships were present in the vicinity of the anomaly at the relevant times. The soundings taken between 0500 and 0600 UTC on 10 January all have a distinct stratospheric intrusion signature between 400 and 250 hPa. Above this feature the profiles once again become characteristic of the troposphere, with moist air, and an almost neutral environmental lapse rate implying

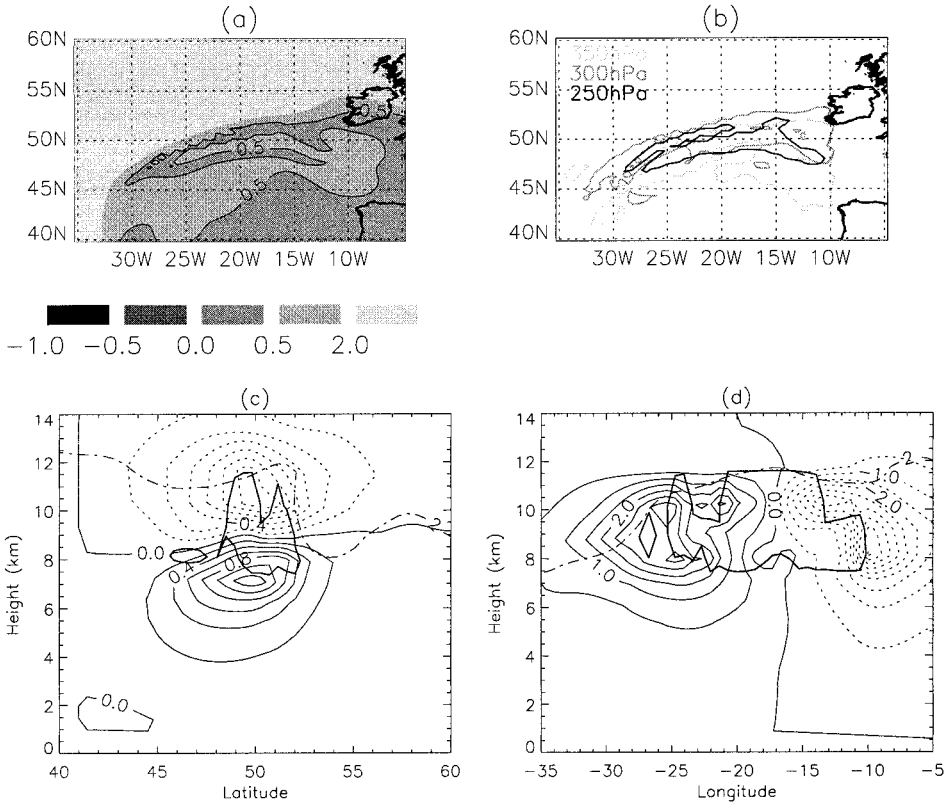

FIG. 7. (a) The PV field after surgery to remove RUPV 2 at 300 hPa at 0600 UTC 10 Jan 1997, (b) −0.1 PVU contour outlining position of PV anomaly. Light gray, 350 hPa; dark gray, 300 hPa; black, 250 hPa. (c) Vertical cross section through anomaly induced potential temperature perturbation at 20°W (contour interval = 0.2 K; positive contours, solid; negative contours, dashed). (d) Vertical cross section through anomaly induced model v component at 49.8°N (contour interval = 0.5 m s^{-1}; positive contours, solid; negative contours; dashed). Bold contour: anomalous PV field = −0.1 PVU. Dotted–dashed contour: PV = 2 PVU contour for unmodified data.

very low PV values. Also the winds at this level are very strong marking the location of the jet stream on the sloping tropopause. It is possible to make an approximation of the PV in the sounding from the ship *Knorr* (41.5°N, 35°W). To gain a horizontal derivative for the wind, the proximity of *Knorr* to the ship *Le Suroit* (40.7°N, 33.5°W) is utilized and a centered difference of the winds calculated. Since the winds from the *Le Suroit* sounding are mainly missing below 450 hPa, the calculation is only performed above this level. The resulting profile is plotted in Fig. 9c overlaid by the profile from the point in the LAM closest to the ships for comparison. Figures 9a and 9b show tephigrams of the soundings from the *Knorr* and *Le Suroit*, respectively.

As a consequence of the much poorer vertical resolution of the LAM data some significant features of the profile are missed, but overall it agrees well with the observations. The ship sounding itself shows typical midtroposphere PV values below about 375 hPa. From 375 to 300 hPa the PV values are very large and characteristic of those found within the stratosphere, agreeing with the hypothesis that this is a tropopause fold. Above 300 hPa a significant region of very low PV is observed. From 250 hPa upward the large PV values indicate the stratosphere. A comparison of the sounding data from *Le Suriot* with the model data also contributes to arguments suggesting that, far from the low PV being a product of model errors, the model significantly underplays the magnitude of the RUPV feature.

5. Analysis of an ILPV anomaly in IOP 1

A third anomaly is defined objectively. Theory concerning diabatic generation of PV anomalies is more certain on the existence of a positive anomaly in the low to middle troposphere than the presence or location of RUPV anomalies. To discuss the evolution of RUPV anomalies and their relative significance in cyclone development, it is useful also to consider their counterpart positive anomalies. Air parcels that reside within RUPV as a result of diabatic heating are likely at some prior stage to have had anomalously high PV, ILPV. The average trajectory of RUPV 1 in Fig. 3 shows an increase in PV value peaking at around 1500 UTC on 9 January.

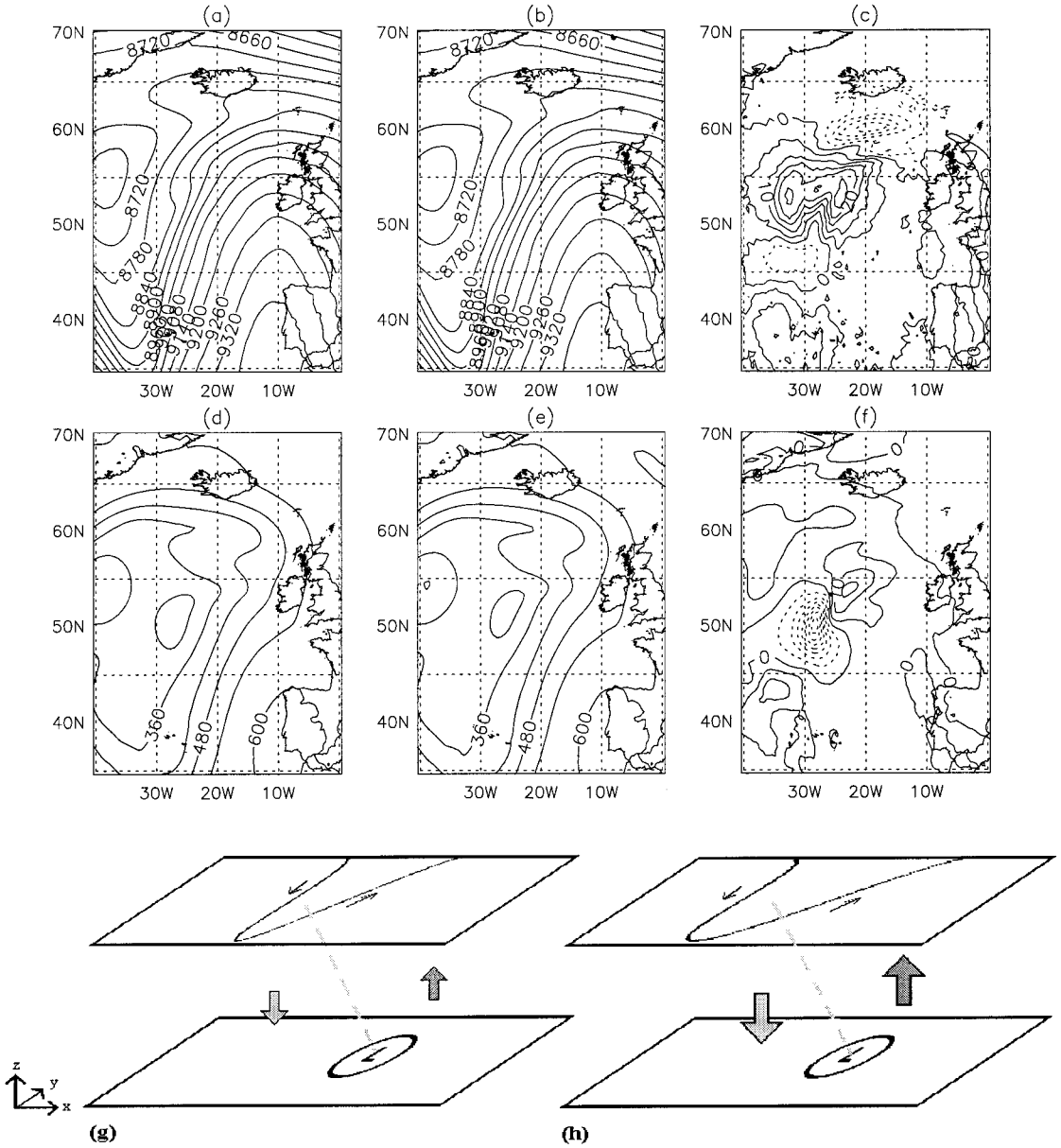

FIG. 8. For 0800 UTC (T + 18) 11 Jan 1997. Top row: 300 hPa. Middle row: 950 hPa. (a) and (d) Geopotential height field from full PV forecast with contour interval = 60 m; (b) and (e) geopotential height field from forecast with RUPV 2 removed with contour interval = 60 m; (c): difference between fields (a) and (b) with contour interval = 5 m; (f): difference between fields (d) and (e) with contour interval = 5 m. Bottom row: schematic demonstrating the differences between the cyclone evolution in (g) the full PV forecast with a thinner upper-level trough, and less vertical motion, and (h) the modified PV forecast with a broader upper-level trough and enhanced vertical motion.

An examination of the positive anomaly, ILPV 1, through which the air parcels in RUPV 1 travel, is undertaken. By examining at 1500 UTC on 9 January the region of increased PV, the objective definition of ILPV 1 could be made (see Table 1). Note that ILPV 1 contains some air parcels that will eventually reside in RUPV 1, but may have, in addition, other heated parcels that do not eventually reside on RUPV 1.

a. Evolution

Figure 10 shows the position of the air parcels belonging to ILPV 1 at 1500 UTC on 9 January at 12 and 24 h before this time, and 0, 12, 24, and, additionally, 30 h later. The contours show the 950-hPa geopotential height. For clarity only those air parcels with PV > 0.5 PVU at 1500 UTC on 9 January 1997 are shown.

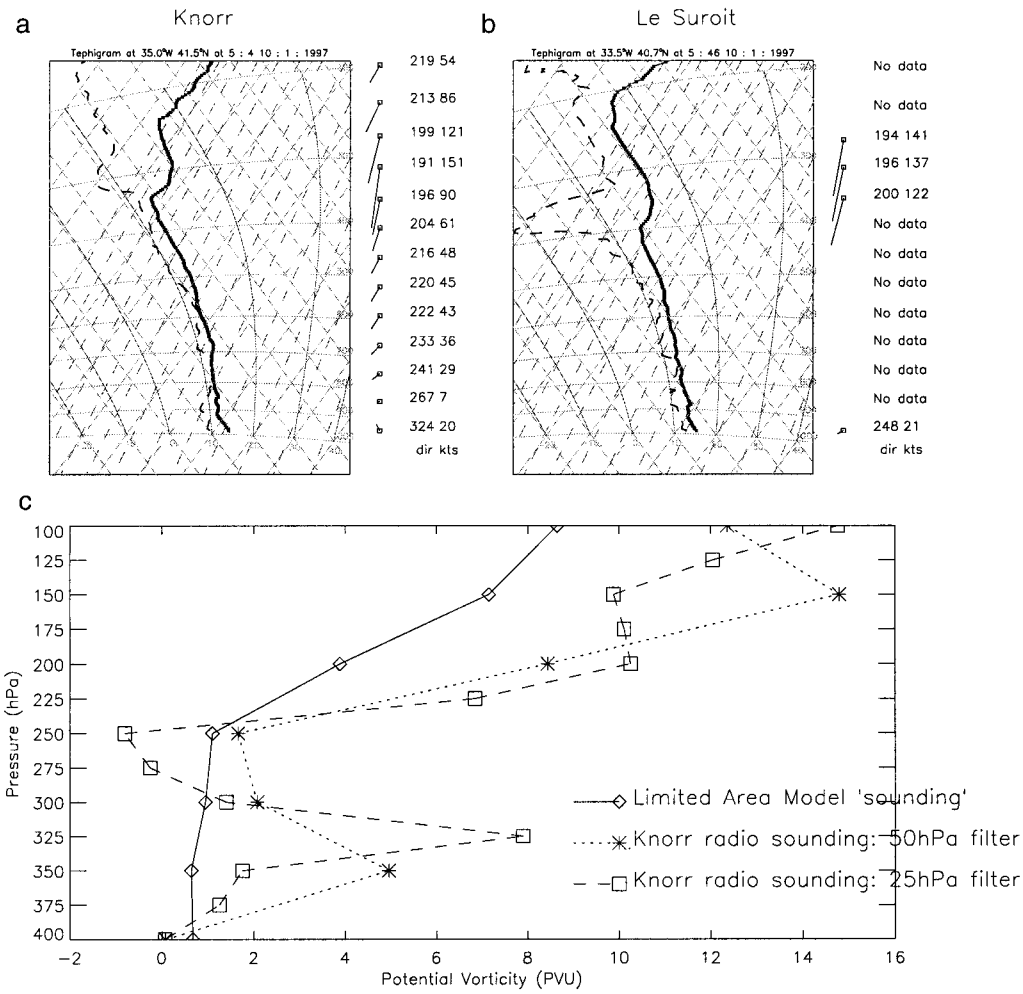

FIG. 9. (a) Tephigram of the *Knorr* sounding at 0504 10 Jan 1997, from 41.5°N, 35°W. (b) Tephigram of the *Le Suroit* sounding at 0546 10 Jan 1997, from 40.7°N, 33.5°W. (c) Calculated PV (PVU) from the two soundings plotted against pressure (hPa). The profile marked with diamonds is the PV from the LAM data at the position of the *Knorr* at 0600 UTC 10 Jan 1997. The profile marked with a dotted line and stars is the PV calculated from the atmospheric sounding data filtered over 50 hPa. The profile marked with a dashed line and squares is the PV calculated from the atmospheric sounding data filtered over 25 hPa. Where insufficient wind data are available to calculate the relative vorticity, a value of f (Coriolis parameter) has been used.

After the anomaly definition time, 1500 UTC on 9 January, differential ascent of air from ILPV 1 is seen. Three distinct paths can be identified: a southerly flow, rising rapidly, a northwesterly flow rising more slowly, and a recirculation within the low. They are defined by their final location and past direction of movement. This prevents biasing the selection of the air flows by their thermodynamic, and physical, characteristics and makes the study of these attributes independent of the airflow definition. The criteria used to define the flows are shown in Table 3.

The three air flows are identified in Fig. 10 by different shades of gray. To illustrate the different properties of the three parts of the flow the average trajectory characteristics have been calculated for each of these airstreams; shown in Fig. 11. They are labeled A (light gray, Fig. 10; short-dashed line, Fig. 11), B (gray, Fig. 10; dotted–dashed line, Fig. 11), and C (black, Fig. 10; long-dashed line, Fig. 11), respectively. A schematic has been constructed of the flow relative to low 8a (Fig. 12), which can be directly compared to the schematic constructed by Young (1994), of the air flow through a depression forming ahead of a strongly diffluent trough. Air flow A can be compared to his W2, air flow B to his W1, and air flow C to his CCB.

Examination of the air parcels within ILPV 1 that become RUPV 1 reveals that these are located on the northern edge of the positive anomaly. They also predominantly, but not exclusively, reside in the lower portion, below 650 hPa. The air within the most leading edge of the anomaly rises most rapidly and, therefore, undergoes the most intense heating and experiences the

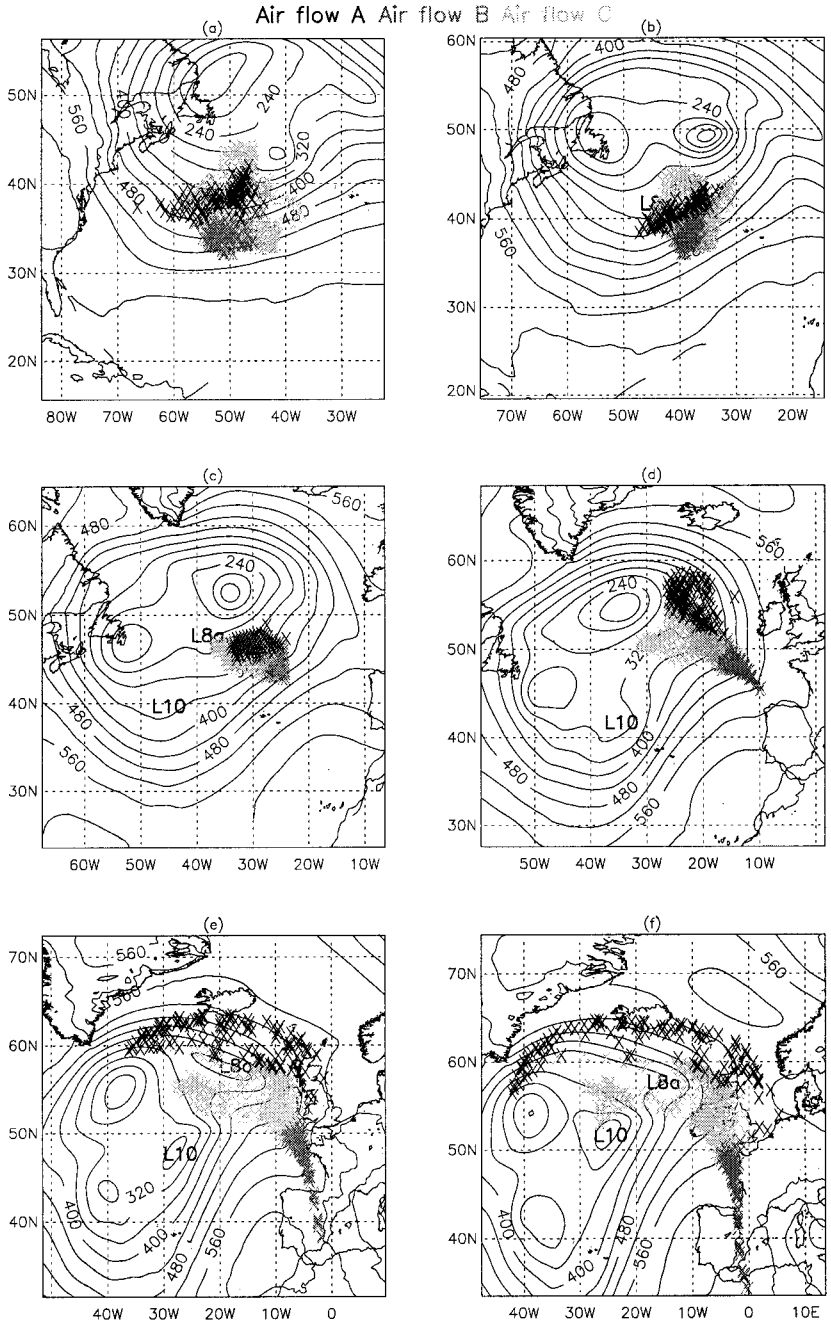

FIG. 10. Contours: 950-hPa geopotential height (contour interval: 40 m). Crosses: location of air parcels; gray shade represents ''air flow''; air parcels belong to A, black; B, dark gray; and C, light gray. See text for more details: (a) 1500 UTC 8 Jan; (b) 0300 UTC 9 Jan; (c) 1500 UTC 9 Jan; (d) 0300 UTC 10 Jan; (e) 1500 UTC 10 Jan; and (f) 2100 UTC.

strongest PV modification, up over the warm front, following the secondary warm conveyor belt flow of low 8a (Carlson 1980; Browning and Roberts 1994). The air parcels continue to be heated diabatically, and a significant proportion become RUPV 1. Subsequently, as described in the investigation into the evolution of RUPV 1, this anomaly is massively strained out along divergent flow of the cloud head. This flow is labeled A in Fig. 12 and in the graphs of the average characteristics. Such a flow has been identified in many previous studies; for example, Kuo et al. (1992) describe an ascending flow that rose from the boundary layer in

TABLE 3. Criteria to define location of air flows. All criteria refer to 10 Jan 1997.

Air flow A	Air flow B	Air flow C
Pressure < 500 hPa at 2100 UTC Latitude at 0600 UTC > latitude at 0900 UTC for air parcels with longitude between 0° and 30°W at 2100 UTC	Latitude at 0600 UTC < latitude at 0900 UTC for air parcels with longitude between 0° and 30°W at 2100 UTC	Pressure > 500 hPa at 2100 UTC Latitude at 0600 UTC > latitude at 0900 UTC

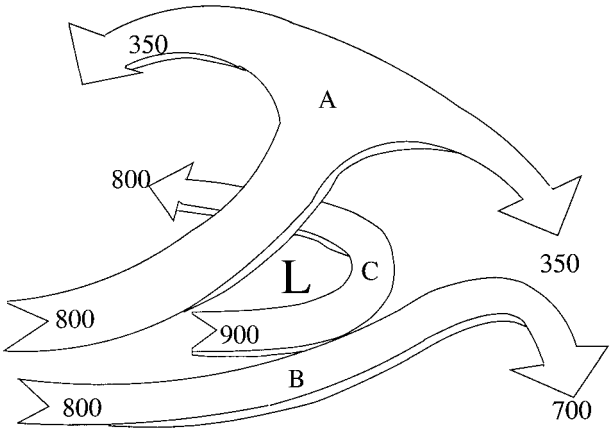

FIG. 12. Schematic diagram of air flow from ILPV 1. The L represents the position of the low center at the final time (2100 UTC 10 Jan 1997). The A is the secondary warm conveyor belt, B the primary warm conveyor belt, and C the recirculation within the low, the cold conveyor belt. The figure shows the pressure (hPa) of the average trajectory at the beginning and end of the air flows. See text for more details.

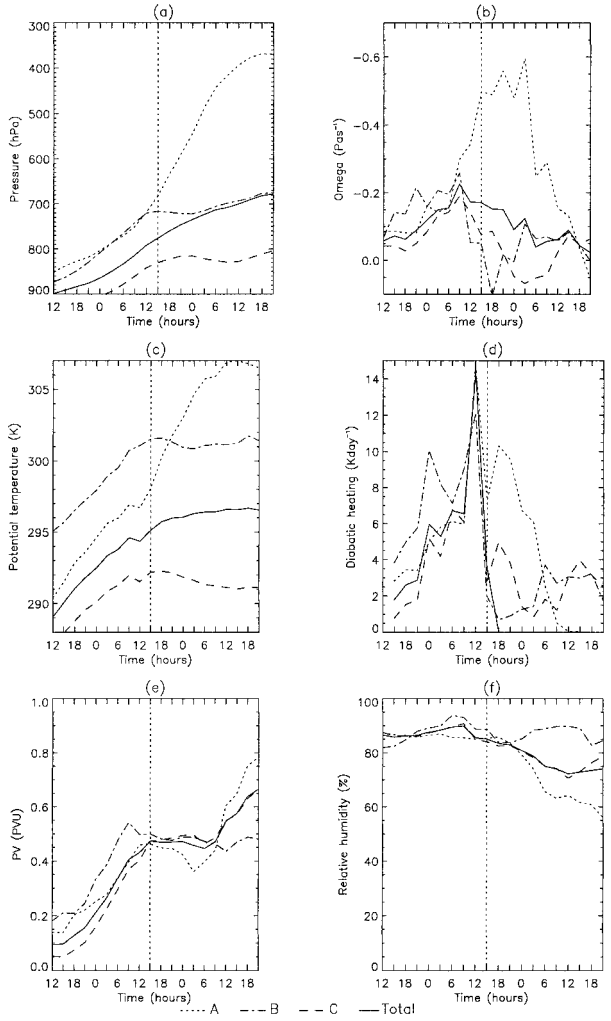

FIG. 11. Characteristics of average trajectory experiencing heating and emanating from ILPV 1. The anomaly definition time is 1500 UTC on 9 Jan 1997 marked by the small dashed vertical line on each graph. The trajectories are calculated from 1200 UTC on 8 Jan to 2100 UTC on 10 Jan; (a) pressure (hPa); (b) vertical velocity (Pa s^{-1}); (c) potential temperature (K); (d) heating (K day^{-1}); (e) potential vorticity (PVU); and (f) relative humidity (%). Solid line corresponds to total flow; short dashes correspond to air flow A; dot–dashes correspond to air flow B; and long dashes correspond to air flow C. See text for explanation.

the vicinity of the warm front and ''spread out in a fan-shaped pattern'' identified using trajectory analysis of a marine cyclone (see in particular their Fig. 16).

A second flow, B, follows the primary warm conveyor belt (Browning 1995), rising more slowly than A, and stemming from the upper half of ILPV 1. The flow travels along the sloping warm front and the PV remains approximately constant. The parcels lie on the frontal surface, and some experience latent heat release within the clouds associated with the warm front. Their average PV remains steady, although this may be a product of the averaging process, as examination of individual air parcels shows the value of PV they attain decreases the higher up the frontal surface they are. Balasubramanian and Yau (1996), when using a three-dimensional primitive equation model to study the development of a moist baroclinic wave cyclone, note ridge intensification by the transport of diabatic RUPV via the warm conveyor belt. Around half of the parcels in ILPV 1 flow out along this southerly path.

The third air flow, C, is a recirculation within the low center along the cold conveyor belt (Carlson 1980; Stewart and Macpherson 1989; Browning 1990; Young 1994). The cold conveyor belt originates ahead of the warm front and ascends along an isentropic surface redistributing moisture within the low. The air flow has the lowest value of wet-bulb potential temperature out of the three. Air parcels remain ''trapped'' within the cyclonic vortex, at around 850–800 hPa. They are steadily heated and their PV continues to rise to 0.66 PVU on average providing the high PV core to the depression. Parcels belonging to C originate from the lower portion of ILPV 1 and make up a third of all the trajectories from ILPV 1.

Each air flow has a distinctive PV evolution signature

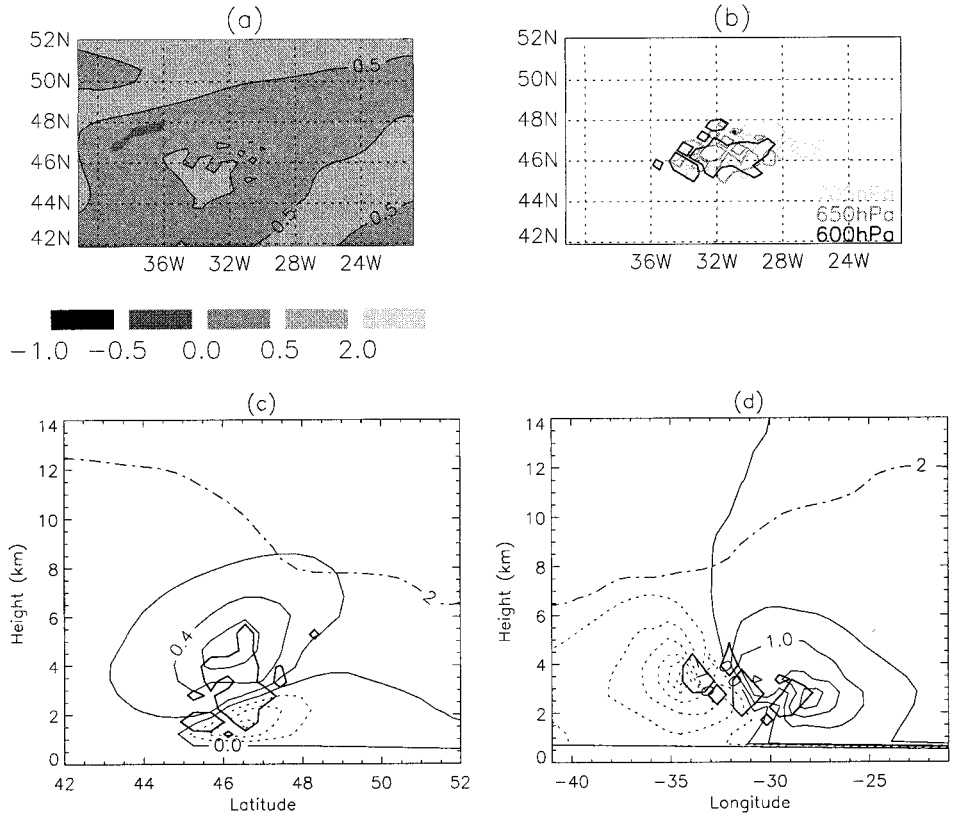

FIG. 13. (a) The PV field after surgery to remove ILPV 1 at 650 hPa, 1500 UTC 9 Jan 1997, (b) 0.1 PVU contour outlining position of PV anomaly. Light gray, 700 hPa; dark gray, 650 hPa, black, 600 hPa. (c) Vertical cross section through anomaly induced potential temperature perturbation at 31.2°W (contour interval = 0.2 K; positive contours, solid; negative contours; dashed). (d) Vertical cross section through anomaly induced model v component at 46.0°N (contour interval = 0.5 m s^{-1}; positive contours, solid; negative contours; dashed). Bold contour: anomalous PV field = 0.1 PVU. Dotted–dashed contour: PV = 2 PVU contour for unmodified data.

that adds dynamical understanding to the conceptual models of conveyor belt flow proposed by Browning and others. Further case studies are required to generalize this result.

b. Inversion

The PV field at 650 hPa after the removal of the anomaly ILPV 1 can be seen in Fig. 13a. Figure 13b shows the resulting anomaly when this field is subtracted from the full PV fields. Figures 13c and 13d show these fields in vertical cross-section with the outline of the anomaly marked by the bold line. See Table 2 for the maximum magnitude of the fields induced by ILPV 1. Figure 13c shows the potential temperature perturbation due to ILPV 1 in a longitudinal section. Theoretical calculations for a positive anomaly show warm temperatures above the anomaly and cold below and this signature is replicated here. The magnitudes of these two temperature anomalies are very similar, with the restriction of constant potential temperature on the bottom boundary of the inversion possibly reducing the strength of the cold anomaly at the surface. The favorably low background PV means the positive temperature anomaly reaches throughout the depth of the troposphere.

Figure 13d shows the component of the wind in an approximately northerly direction as induced by the anomaly. As expected for a positive anomaly a cyclonic flow is seen around the anomaly. Again these fields stretch throughout the troposphere, and the discontinuities at around 0.75 km are due to the imposition of the original wind field below 900 hPa subsequent to the inversion, while no restriction is placed on the wind at the bottom boundary (at 900 hPa) during the inversion.

c. Rerun

To calculate the atmospheric response to the anomaly ILPV 1 defined at 1500 UTC on 9 January, two model forecasts were generated. The first of these was a rerun of the LAM from 1200 UTC on 9 January, which stopped at 1500 UTC and restarted with the fields from an inversion of the full PV field. The second was re-

started using fields from the inversion of the PV field generated by removing objectively defined ILPV 1. A subarea of this field at 650 hPa is illustrated in Fig. 13b. The modified PV forecast lags the full PV field forecast in developing low 8a, in both speed of propagation and the depth of the low.

These observations support the hypothesis that positive lower-troposphere anomalies increase the propagation speed and also the low-level circulation of their parent cyclone. Examination of the surface thermal structure fails to provide clear evidence of an exaggerated signal in the full PV forecast in comparison to the other run. The deeper development of low 8a in the presence of the anomaly may suggest that coupling is better between upper and lower levels of the troposphere in the full run. However no significant modification of the upper levels is revealed in the modified PV field forecast.

Investigation of the evolution of ILPV 1 using the analysis data revealed that three air flows stemmed from it. The first of these resulted in RUPV 1. An anomaly occupying a very similar position and magnitude can be seen in both forecasts at around 0300 UTC on 10 January. This suggests the continued development of the low is only delayed and not changed fundamentally in character.

6. Conclusions

The dynamical role of RUPV anomalies within a cyclone system has been studied by examining the objectively defined anomalies within IOP 1 of FASTEX. An understanding of the influence of such anomalies is important in helping to complete the conceptual PV picture of a cyclone.

a. How does reduced upper-tropospheric PV evolve?

By considering trajectories from the two objectively defined RUPV anomalies from IOP 1 the evolution of each could be studied in terms of the origin, physical characteristics, and modification over time of the air parcels that reside within each anomaly at the definition time. This showed a gradual increase in the PV of the air parcels until the level of maximum heating was reached and then a decrease in PV over time was recorded. This is in broad agreement with the theoretical modification of PV as proposed in Wernli's (1995) model. An additional decrease in PV was also seen after the parcels had left the influence of the heating, which is not explicitly accounted for in their theory. This ''disparity'' was explored by considering the evolution of the air flow away from the positive diabatic anomaly ILPV 1. Three distinct air flows were identified as shown schematically in Fig. 12.

Air flow A resulted in RUPV 1, and air flow B followed the line of the warm conveyor belt above the warm front experiencing a small decrease in PV. Air flow C remained within the low center recirculating around the core of the depression and increasing steadily in PV magnitude. These trajectories found moving through and with low 8a agree remarkably well with those calculated by Golding (1984) for an idealized simulation of baroclinic wave development. Here none of these flows experience the extreme scenario of steady heating and continuous ascent forming a midlevel positive PV anomaly at the center of the low, even though one forms through the action of the recirculation following the cold conveyor belt. A steady state, such as Wernli and Davies require, is not seen in this low pressure system. Cyclones rapidly evolve and develop, with control switching between upper and lower levels, frontogenesis creating important secondary circulations, and the strength of latent heat release varying temporally and spatially. These factors allow the formation of RUPV anomalies. It is therefore important to note that, when considering the models of Kleinschmidt and of Wernli and Davies, the conditions under which each of these extremes is valid rarely exist in the atmosphere. The modification of PV due to diabatic processes lies along a continuous spectrum, the two extremes of which are the models of Kleinschmidt and of Wernli and Davies. For the case study examined here air flow B experiences an increase and a decrease in PV similar to the steady-state model. RUPV 1 is formed due to strong heating during the initial development of the low with more similarities to the instantaneous heating model.

b. How important is reduced upper-tropospheric PV in midlatitude cyclone genesis and evolution, particularly in comparison to increased lower-tropospheric PV anomalies also created by diabatic processes?

1) INSTANTANEOUS

The maximum potential temperature anomaly and wind speed attributable to a RUPV anomaly was compared with the total variation within the inversion domain at that time and on the appropriate pressure surface. Anomaly RUPV 2 induced marginally both the largest wind (13%) and temperature fields (7%), and ILPV 1 the smallest wind (10%) and temperature fields (4%). RUPV 1 had the same maximum magnitude to ILPV 1 but was of opposite sign, and induced larger perturbations, agreeing with theoretical results suggesting that negative anomalies induce larger fields. The influence of the proximity of the tropopause was also seen for the ''real'' anomalies, with reduced upward penetration of fields into the stratosphere. In general the results suggested that the largest influence could be affected by RUPV 2. The position of this anomaly with respect to the cyclone and its proximity to the sharp tropopause cliff are also factors promoting its importance.

Past work has centered on the role of the apparently

larger and more powerful positive lower-tropospheric anomaly. One of the overall aims of this study is to test the assumption that the positive anomaly is more important. By performing a comparison of the *instantaneous* influence of these two types of anomaly upon the parent cyclone, the information available from the numerical calculations, it has been shown that it is not valid to neglect the role of the negative anomaly in comparison to the positive anomaly.

2) EVOLUTION

To determine the temporal role of RUPV anomalies in the development of their parent cyclone, and other cyclones within their influence, reruns of the Limited Area Model were performed. This was also done for ILPV 1. It was shown that RUPV 1 did not have an important role to play in the subsequent evolution of the parent depression, low 8a, or that of any downstream system. Conversely, RUPV 2 played an important role in curtailing the development of low 10, its parent low. When RUPV 2 was removed from the forecast run at 0600 UTC on 10 January reduced anticyclonic curvature in the upper-level ridge allowed the trough to broaden eastward. Thorncroft et al. (1993) within the context of their examination of ''anticyclonic'' and ''cyclonic'' life cycles consider the effects of trough thinning, as under a mean anticyclonic shear, and trough broadening under a mean cyclonic shear. They call upon the ''scale effect'' described by Hoskins et al. (1985) to explain how the thinner the trough is the more passive it becomes. Considering the upper-level trough as a large PV anomaly, this is deducible from scaling arguments applied to the inverse Laplacian, a smoothing operator. A larger trough is therefore more dynamically active, inducing larger vertical velocities, and exhibiting a more favorable tilt between upper and lower levels. Although it is not possible to say that the absence of RUPV 2 implies a cyclonic shear, trough broadening of approximately 400 km is seen toward the east in the second forecast. As a result of the position of the upper-level trough relative to the depression, coupling between upper and lower levels is enhanced. A schematic of these interactions is presented in Figs. 9g and 9h. Davies et al. (1996) have reached similar conclusions to Thorncroft et al. in their study of baroclinic wave development under cyclonic and anticyclonic barotropic shear. The cyclonic shear creates a stronger surface low, and under anticyclonic conditions the westward tilt with height increases over time, rather than decreasing as would be expected in a rapidly developing midlatitude depression. They also comment on the ability to create substantial changes in cyclone evolution with relatively small changes in the background state. The absence of RUPV 2 appears to delay the early development of the low and allows more favorable atmospheric conditions to exist for rapid growth of a possibly more powerful frontal wave cyclone. Additional analysis was undertaken comparing a full LAM forecast from 0000 UTC on 9 January 1997 to the analysis to establish the dynamical consistency of the analyzed data fields used throughout this study. Both lows 8a and 10 were more vigorous in the forecast run, and this is reflected in the different positions of the RUPV features seen with respect to the parent lows and the upper-level features. Conclusions that can be drawn from these results agree well with those more rigorously obtained as described above.

The rapid reformation of ILPV 1 after removal meant any influence of the anomalies *absence* was small and swiftly dissipated. As expected a reduction in the propagation speed *was* seen, as were initial decreases both in the low-level circulation and in the depth of the depression. However no significant effects were recorded in the subsequent evolution of low 8a, and a similar anomaly to RUPV 1 formed.

Here it has been seen how the short-term production of RUPV 2 early on by low 10 reduced the parent cyclone's later development, while when RUPV 2 was absent a tighter, possibly more rapidly developing, low appeared.

c. Is the presence of RUPV within numerical model analyses validated?

Atmospheric profiles from the radiosonde measurements in FASTEX showed extraordinary evidence of very low static stability in the upper-troposphere indicative of low PV and also showed the signature of a tropopause fold. An example of these excellent data is shown in Fig. 5. Comparisons of these results with those from the model indicate that the model does not do full justice to the magnitude of the RUPV anomalies.

Case study work has been undertaken to isolate and define reduced upper-tropospheric PV anomalies, and then to examine their dynamical evolution and influence on their surroundings. Instantaneously such anomalies induce *nonnegligible* perturbations to the geopotential field, which are of at least equal magnitude to diabatically produced increased lower-tropospheric PV anomalies. Their influence over time in the case study investigated here is apparently small. However their maximum impact seemingly comes during the initial development of the low and, therefore, can play a *vital* role in the long-term evolution of the cyclone. This is in contrast to the diabatically produced positive PV anomaly that is most ''powerful'' in the later stages of the cyclone development. Observations have been presented that show that reduced upper-tropospheric PV is a significant phenomenon in the atmosphere. It is important to carry out further case studies having set the scene with this initial study, and recognizing the limitations of the model dataset used here analysis at higher resolution would be insightful.

Acknowledgments. The authors wish to thank Dr. Sid

Clough for his encouragement and input. Hannah Pomroy was in receipt of a NERC CASE research studentship; the CASE partner being the U.K. Meteorological Office. We also thank Dr. Morwenna Griffiths for her helpful comments concerning PV inversion and the Limited Area Model, Dr. Ed Dicks for programming assistance, Dr. Heini Wernli for the use of his trajectory code, and Michal Ziemianski for use of the nonlinear balance inverter code.

REFERENCES

Balasubramanian, G., and M. K. Yau, 1996: The life cycle of a simulated marine cyclone: Energetics and potential vorticity diagnostics. *J. Atmos. Sci.,* **53,** 639–653.

Birkett, H. R., 1998: Reduced upper-tropospheric potential vorticity. Ph.D. thesis, Department of Meteorology, University of Reading, 190 pp. [Available from Dept. of Meteorology, University of Reading, Reading RG6 6BB, United Kingdom.]

——, and A. J. Thorpe, 1997: Superposing semi-geostrophic potential vorticity anomalies. *Quart. J. Roy. Meteor. Soc.,* **123,** 2157–2163.

Bishop, C. H., and A. J. Thorpe, 1994: Potential vorticity and the electrostatics analogy: Quasi-geostrophic theory. *Quart. J. Roy. Meteor. Soc.,* **120,** 713–731.

Browning, K. A., 1990: Organisation of clouds and precipitation in extratropical cyclones. *Extratropical Cyclones: The Erik Palmén Memorial Volume,* C. Newton and E. O. Holopainen, Eds., Amer. Meteor. Soc., 129–154.

——, 1995: Mesoscale aspects of extratropical cyclones: An observational perspective. JCMM Internal Rep. 44, 60 pp. [Available from JCMM, University of Reading, Reading RG6 6BB, United Kingdom.]

——, and N. M. Roberts, 1994: Structure of a frontal cyclone. *Quart. J. Roy. Meteor. Soc.,* **120,** 1535–1557.

Carlson, T. N., 1980: Airflow though mid-latitude cyclones and the comma cloud pattern. *Mon. Wea. Rev.,* **108,** 1498–1509.

Clough, S. A., and Coauthors, 1998: A JCMM overview of FASTEX intensive observing periods. JCMM Internal Rep. 81, 60 pp. [Available from JCMM, University of Reading, Reading, RG6 6BB, United Kingdom.]

Cullen, M. J. P., 1993: The unified forecast/climate model. *Meteor. Mag.,* **122,** 81–94

Davies, H. C., Ch. Schär, and H. Wernli, 1991: The palette of fronts and cyclones within a baroclinic wave development. *J. Atmos. Sci.,* **48,** 1666–1689.

Davis, C. A., 1992: A potential vorticity diagnosis of the importance of initial structure and condensational heating in observed extratropical cyclogenesis. *Mon. Wea. Rev.,* **120,** 2409–2428.

——, and K. A. Emanuel, 1991: Potential vorticity diagnostics of cyclogenesis. *Mon. Wea. Rev.,* **119,** 1929–1953.

——, M. T. Stoelinga, and Y.-H. Kuo, 1993: The integrated effect of condensation in numerical simulations of extratropical cyclogenesis. *Mon. Wea. Rev.,* **121,** 2309–2330.

——, E. D. Grell, and M. A. Shapiro, 1996: Balanced dynamical nature of a rapidly intensifying oceanic cyclone. *Mon. Wea. Rev.,* **124,** 3–26.

Demirtas, M., and A. J. Thorpe, 1999: Sensitivity of short-range weather forecasts to local PV modifications. *Mon. Wea. Rev.,* **127,** 922–939.

Golding, B. W., 1984: A study of the structure of mid-latitude depressions in a numerical model using trajectory techniques. I: Development of ideal baroclinic waves in dry and moist atmospheres. *Quart. J. Roy. Meteor. Soc.,* **110,** 847–879.

Griffiths, M., A. J. Thorpe, and K. A. Browning, 1999: Convective destabilisation by a tropopause fold diagnosed using potential vorticity inversion. JCMM Internal Rep. 96, 48 pp. [Available from JCMM, University of Reading, Reading RG6 6BB, United Kingdom.]

Haynes, P. H., and M. E. McIntyre, 1987: On the evolution of vorticity and potential vorticity in the presence of diabatic heating and other forces. *J. Atmos. Sci.,* **44,** 828–841.

——, and ——, 1990: On the conservation and impermeability theorems for potential vorticity. *J. Atmos. Sci.,* **47,** 2021–2031.

Hoskins, B. J., 1991: Towards a PV–θ view of the general circulation. *Tellus,* **43AB,** 27–35.

——, M. E. McIntyre, and A. W. Robertson, 1985: On the use and significance of isentropic potential vorticity maps. *Quart. J. Roy. Meteor. Soc.,* **111,** 877–946.

Joly, A., and Coauthors, 1997: The Fronts and Atlantic Storm Track Experiment (FASTEX): Scientific objectives and experimental design. *Bull. Amer. Meteor. Soc.,* **78,** 1917–1940.

Kleinschmidt, E., 1950: On the structure and origin of cyclones: Part II. *Meteor. Rundsch.,* **3** (3/4), 54–61. [U. K. Met. Office Transl. 1701.]

Kuo, Y.-H., R. J. Reed., and S. Low-Nam, 1992: Thermal structure and airflow in a model simulation of an occluded marine cyclone. *Mon. Wea. Rev.,* **120,** 2280–2297.

Persson, P. O. G., 1995: Simulations of the potential vorticity structure and budget of FRONTS 87 IOP8. *Quart. J. Roy. Meteor. Soc.,* **121,** 1041–1081.

Petterssen, S., 1956: *Weather Analysis and Forecasting.* Vol. I, *Motion and Motion Systems,* McGraw-Hill, 428 pp.

Reed, R. J., M. T. Stoelinga, and Y.-H. Kuo, 1992: A model-aided study of the origin and evolution of the anomalously high potential vorticity in the inner region of a rapidly deepening marine cyclone. *Mon. Wea. Rev.,* **120,** 893–913.

Seibert, P., 1993: Convergence and accuracy of numerical methods for trajectory calculations. *J. Appl. Meteor.,* **32,** 558–566.

Stewart, R. E., and S. R. Macpherson, 1989: Winter storm structure and melting-induced circulations. *Atmos.–Ocean,* **27,** 5–23.

Stoelinga, M. T., 1996: A potential vorticity-based study of the role of diabatic heating and friction in a numerically simulated baroclinic cyclone. *Mon. Wea. Rev.,* **124,** 849–874.

Thorncroft, C. D., B. J. Hoskins, and M. E. McIntyre, 1993: Two paradigms of baroclinic-wave life-cycle behaviour. *Quart. J. Roy. Meteor. Soc.,* **119,** 17–55.

Thorpe, A. J., and C. H. Bishop, 1995: Potential vorticity and the electrostatics analogy: Ertel–Rossby formulation. *Quart. J. Roy. Meteor. Soc.,* **121,** 1477–1495.

Wernli, H., 1995: Lagrangian perspective of extratropical cyclogenesis. Ph.D. thesis, ETH Zürich, Zurich, Switzerland, 157 pp. [Available from Swiss Federal Institute of Technology, ETH Zentrum, CH-8092 Zurich, Switzerland.]

——, and H. C. Davies, 1997: A Lagrangian based analysis of extratropical cyclones: The method and some applications. *Quart. J. Roy. Meteor. Soc.,* **123,** 467–490.

Whitaker, J. S., L. W. Uccellini, and K. F. Brill, 1988: A model-based diagnostic study of the rapid development phase of the Presidents' Day cyclone. *Mon. Wea. Rev.,* **116,** 2337–2365.

Young, M. V., 1994: A classification scheme for cyclone life-cycles: Applications in analysis and short-period forecasting. *Life Cycles of Extratropical Cyclones,* Vol. III, Bergen, Norway, Institute of Geophysics, University of Bergen, 380–385.

Ziemianski, M., 1994: Potential vorticity inversion. JCMM Internal Rep. 39, 22 pp. [Available from JCMM, University of Reading, Reading RG6 6BB, United Kingdom.]